MPPT for Electromagnetic Energy Harvesters Having Nonnegligible Output Reactance Operating Under Slow-Varying Conditions

Kimberley Hiu-kwan Tse, *Student Member, IEEE*, and Henry Shu-hung Chung, *Fellow, IEEE*

***Abstract*—Most maximum power point trackers (MPPTs) for electromagnetic energy harvesters (EMEHs) are based on resistive matching technology, where the input resistance of the MPPT is made equal to the magnitude of the output impedance of the harvester. This is valid when the output reactance of the EMEH is much smaller than its output resistance. However, some EMEHs, such as permanent magnet generator, have nonnegligible output reactance. The discrepancy between the power extracted by the resistive matching technology and the maximum extractable power will increase as the output reactance increases. Under high excitation frequency and low operating temperature, the effect of the output reactance will become more dominant. In order to deal with such issue, an MPPT that can counteract the effect of the coil inductance and match with the coil resistance is presented. It does not require knowing coil parameters *a priori* and the harvester will be operated at its true maximum power point. A 7-W prototype for testing the proposed algorithm has been built and evaluated. Its performance is favorably compared with the amount of power extracted with the resistive matching technology.**

***Index Terms*—Electromagnetic energy harvesters (EMEHs), energy harvesting, impedance matching, maximum power point tracking (MPPT).**

I. Introduction

RECENT advances in semiconductor technology and material sciences have reduced the power consumption of modern microelectronic circuits and systems, such as Internet-of-Things and machine-to-machine devices, and have also enhanced the conversion efficiency from ambient energy into electricity. The goal of energy harvesting is to replace batteries or extend the recharge intervals of batteries. Among various ambient energy sources, vibration energy harvesting owns the merits of being stable, clean, high power density, and its compatibility with microfabrication.

Manuscript received July 23, 2019; revised October 25, 2019; accepted December 4, 2019. Date of publication December 11, 2019; date of current version March 13, 2020. This work was supported by a grant from the Research Grants Council of the Hong Kong Special Administrative Region, China, under Project 11205418. This paper was presented in part at the IEEE Energy Conversion Congress and Exposition, Cincinnati, OH, USA, Oct. 2017 [37]. Recommended for publication by Associate Editor O. C. Onar. *(Corresponding author: Henry Shu-Hung Chung.)*

The authors are with the Centre for Smart Energy Conversion and Utilization Research, Department of Electrical Engineering, City University of Hong Kong, Hong Kong (e-mail: hiuktse3-c@my.cityu.edu.hk; eeshc@cityu.edu.hk).

Color versions of one or more of the figures in this article are available online at http://ieeexplore.ieee.org.

Digital Object Identifier 10.1109/TPEL.2019.2959625

The power level of vibrational and rotational electromagnetic energy harvesters (EMEHs) ranges from several tens of μW to kW in applications, such as wearable devices [1], [2], knee-mounted biomechanical energy harvesters [3], vehicle suspensions [4], ocean wave energy conversion [5], etc. An energy harvesting system is composed of three main components. They are energy harvester, ac/dc converter, and load with or without energy storage element [6].

The operation of the energy harvester is based on the principle of electromagnetic induction with movable magnet(s) and/or copper coils to produce electricity by varying the magnetic flux linkage on the coils [7], [8]. Various structures have been proposed. They differ in size, form factor, magnet material, coupling mechanism, excitation condition, and output performance. Many architectures, mechanical designs, modeling, and optimization techniques have been proposed [9].

The ac/dc converter is used to convert the harvested ac power into dc power. Its input characteristic is controlled to match with the output characteristic of the harvester so that the power extracted from the harvester is maximized. The ac/dc converter typically comprises two main parts: 1) power processing circuit and 2) controller. Much research has been devoted to developing topologies for the power processing circuit and algorithms for operating the harvester at the maximum power point (MPP). Fig. 1 shows the classifications.

The simplest form of ac/dc converter is half-wave or full-wave rectifier having an output capacitor [10]–[12]. Its input resistance is primarily determined by the circuit components and the load. In order to control the input resistance, a dc/dc converter is sometimes connected to the output of the rectifier to regulate its input voltage, current, or power [11]–[17]. Some topologies have the front-end diode bridge replaced by an active bridge for increasing energy efficiency [1].

Some direct ac/dc converters have been proposed to eliminate the power loss of the diode bridge. Refs. [18] and [19] have proposed dual-polarity boost and buck-boost converters, where two converters are operated complementarily. One of them is operated in the positive half cycle of the harvested ac power, while the other one is operated in the negative half cycle. In [20], [21], a hybrid boost and buck-boost converter is proposed. It is operated as a boost converter in the positive half cycle and as a buck-boost converter in the negative half cycle.

In [10], [21]–[26], two-quadrant boost converters with secondary-side diode/switch-based converter, or split capacitor

0885-8993 © 2019 IEEE. Personal use is permitted, but republication/redistribution requires IEEE permission.
See https://www.ieee.org/publications/rights/index.html for more information.

Authorized licensed use limited to: Chulalongkorn University provided by UniNet. Downloaded on August 25,2020 at 06:24:19 UTC from IEEE Xplore. Restrictions apply.

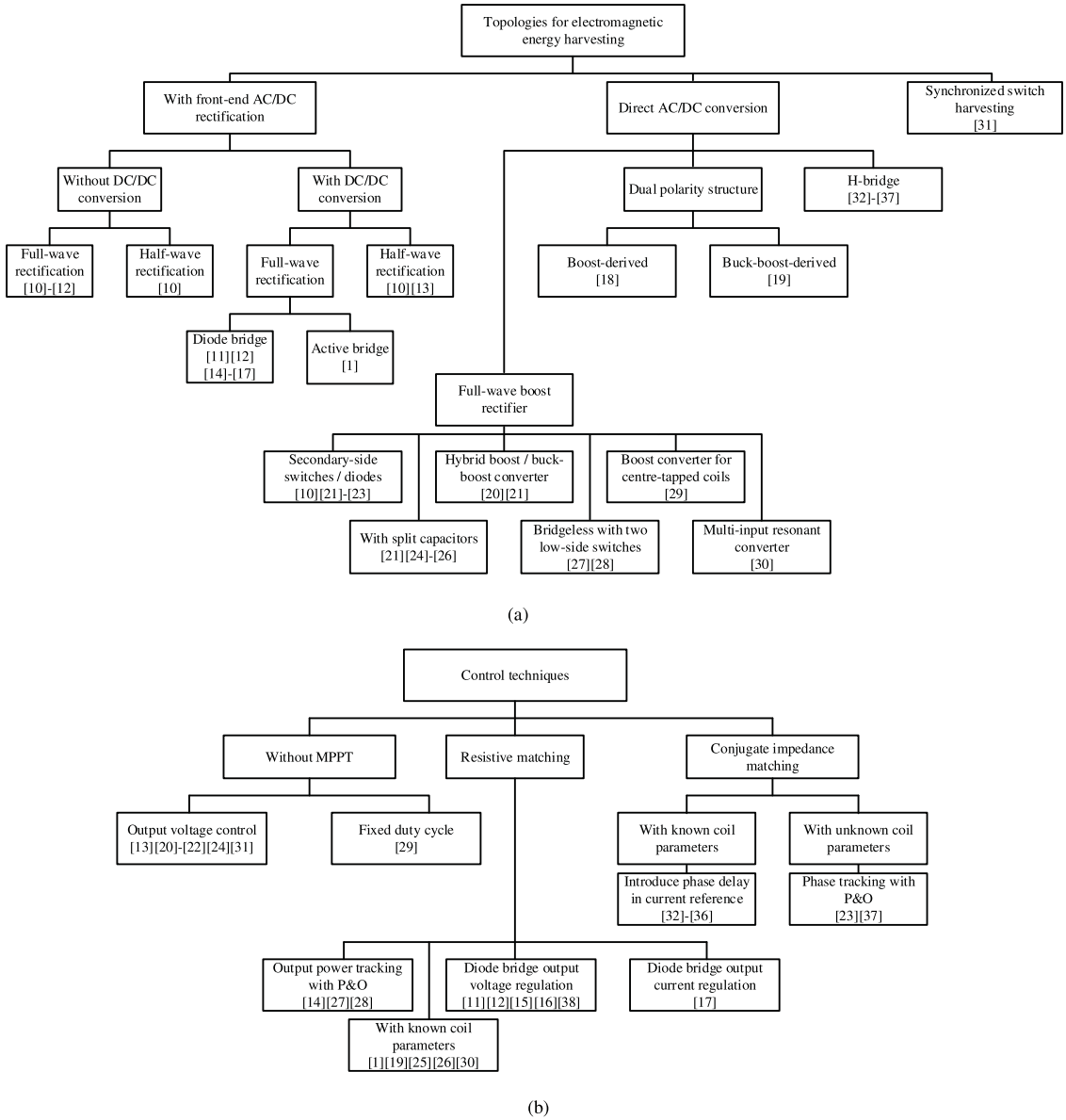

Fig. 1. Classifications of electromagnetic energy harvesting techniques. (a) Power processing circuits. (b) Control techniques.

-based topology are proposed. The coil inductance of the harvester is used as the boost inductor. After charging up the inductance through a bidirectional switch, the energy stored in the inductance is transferred to the load together with the energy generated by the source through the output diode/switch network or split capacitor network. Some buck-boost-derived structures have been discussed in [21]. By extending the concept, nonsynchronous boost converter with two low-side switches has been proposed in [27], [28]. Since the abovementioned converters are all operated in discontinuous conduction mode (DCM), the output current of the harvester is in phase with the open-circuit voltage of the harvester.

Some topologies are designed for specific structure and arrangement of harvester(s) and energy transfer profile. In [29], a single boost converter that connects alternately to the two windings of a center-tapped coil via two series diodes has been proposed. In [30], a resonant converter for multiple harvesters has been proposed. In [31], a synchronized switch harvesting topology, which is based on the power processing technique for piezoelectric harvesters, has been proposed. Finally, in [32]–[37], an H-bridge is used to synthesize a complex load on the harvester.

Many ac/dc converters do not incorporate MPP tracking function [13], [20]–[22], [24], [31]. They perform output voltage regulation or have the main switch operated at a fixed duty cycle [29]. Many techniques are dominantly based on resistive matching. Since the input characteristic of the power processing circuit is resistive, it is controlled to match with the magnitude of the output impedance of the harvester. In [14], [27], [28], the MPP is located by maximizing the output power of the harvester with a perturb-and-observe (P&O) method. In [11], [12], [15]–[17], [38], the output voltage or output current of the

Authorized licensed use limited to: Chulalongkorn University provided by UniNet. Downloaded on August 25,2020 at 06:24:19 UTC from IEEE Xplore. Restrictions apply.

diode bridge is regulated at an optimal value. In [1], [19], [25], [26], [30], the MPP is located with the coil resistance known *a priori*.

In principle, in order to operate the harvester at the true maximum power point (TMPP), the input impedance of the ac/dc converter should be equal to the complex conjugate of the output impedance of the harvester [39]. More specifically, the output current has to be in the same phase and wave shape as the open-circuit voltage of the harvester. In [32]–[36], with known coil parameters, a complex load impedance is synthesized by an H-bridge and a phase delay introduced in the current reference. Ref. [36] gives a general model for explaining the need of counteracting the effect of the output reactance. However, the intrinsic parameters of the harvesters and resonant frequency have to be determined *a priori*, so that the values of the complex impedance for single or multiple resonant frequencies are precalculated. In [23], a phase tracking technique with a P&O method for unknown coil parameters is proposed. Sinusoidal excitation is assumed in the implementation.

A maximum power point tracker (MPPT) that can locate the TMPP is presented. It is an extension of the prior work in [37]. The power processing circuit is an H-bridge, where the current stress is lower than the topologies operating in DCM, thus, suitable for high-power energy harvesting. The controller does not require knowing the values of the coil resistance and coil inductance *a priori*. The input impedance of the H-bridge is controlled to behave like a frequency-dependent capacitor with a series resistor. The equivalent capacitance is used to counteract the effect of the output inductance of the harvester, while the equivalent resistance is used to match the output resistance of the harvester. The excitation is not restricted to sinusoidal profile. A 7-W prototype MPPT has been built and evaluated. Its performance is favorably compared with the amount of power extracted with the resistive matching technique.

II. Effect of the Output Inductance on Power Extraction

An EMEH is modeled by a Thevenin's equivalent circuit consisting of an ideal voltage source v_T and an output impedance Z_T [6], [13], [31], [39], [40]. It is shown in Fig. 2. v_T represents the total voltage induced in the coil(s). Z_T consists of two components, including an equivalent output resistance R_T and equivalent output inductance L_T. As the excitation frequency is low, R_T is highly dependent on the operating temperature. Thus, R_T can be approximated by

$$R_T(T) = R_T(T_0)\ (1 + \alpha\ \Delta T) \tag{1}$$

where $R_T(T_0)$ is the value of R_T at the reference temperature T_0, α is the temperature coefficient, and $\Delta T = T - T_0$ is the temperature difference.

The value of α of copper is 0.00386 Ω/°C, implying that R_T increases by 3.86% for every 10 °C increase in the operating temperature. The value of L_T is sometimes frequency dependent. Thus, Z_T can be modeled by

$$Z_T(T,\ f) = R_T(T) + j\ X_T(f) \tag{2}$$

where $X_T(f) = 2\ \pi\ f\ L_T(f)$ and f is the excitation frequency.

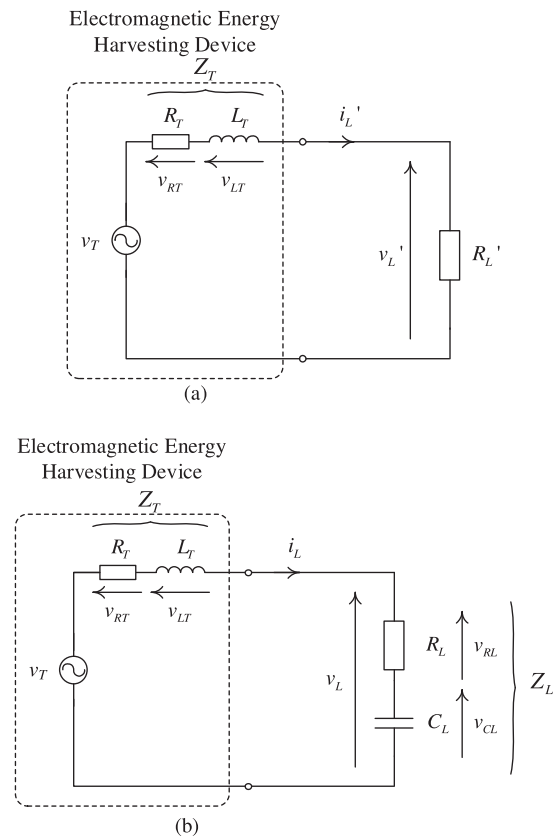

Fig. 2. Equivalent circuit with different types of load. (a) With resistive load. (b) With capacitive load.

The amount of power transferred from the harvester to a load depends on the type and value of the load. As discussed in [41], if the load is resistive, i.e., R_L' in Fig. 2(a), maximum power transfer occurs when

$$R_L'(T,\ f) = \sqrt{{R_T}^2(T) + [\omega\ L_T(f)]^2} \tag{3}$$

where $\omega = 2\ \pi\ f$.

Such condition is equivalent to the operation when the harvester is connected to a dc/dc converter through a diode bridge with power factor correction, where the load current i_L' is in phase with the load voltage v_L'. The amount of power delivered to R_L', P_L' is

$$P_L'(T,\ f) = \frac{{V_T}^2}{[R'_L(T,\ f) + R_T(T)]^2 + [\omega\ L_T(f)]^2} \times R_L'(T,\ f) \tag{4}$$

where V_T is the root-mean-square (rms) value of v_T.

Hence, P_L' is dependent on the excitation frequency and operating temperature, but the harvester is not operated at the TMPP. To make the extracted power be independent on the excitation frequency, the load should be able to eliminate the effect of the output inductance. The load has to satisfy two requirements: 1) the load current should be in phase with v_T, instead of the load voltage, and 2) the output current should be of the same waveshape as v_T. As illustrated in Fig. 2(b), the load Z_L should

Authorized licensed use limited to: Chulalongkorn University provided by UniNet. Downloaded on August 25,2020 at 06:24:19 UTC from IEEE Xplore. Restrictions apply.

be the complex conjugate of Z_T. That is,

$$Z_L(T,\ f) = R_L(T) + X_L(f) \tag{5}$$

where $R_L(T) = R_T(T)$ and $X_L(f) = -X_T(f)$.

At TMPP, the load current $i_{L,\mathrm{TMPP}}$ and the load power $P_{L,\mathrm{TMPP}}$ are

$$i_{L,\mathrm{TMPP}}(T) = \frac{V_T}{2\ R_T(T)} \tag{6}$$

$$P_{L,\mathrm{TMPP}}(T) = \frac{{V_T}^2}{4\ R_T(T)}. \tag{7}$$

Thus, as Z_T is inductive, Z_L should be capacitive. Let C_L be the equivalent capacitance. Since X_T is frequency dependent, C_L should also be frequency dependent. Based on (5), the reactance of L_T is the same as the reactance of C_L. Thus,

$$\frac{1}{2\ \pi\ f\ C_L(f)} = 2\ \pi\ f\ L_T(f)$$
$$\Rightarrow C_L(f) = \frac{1}{4\ \pi^2\ f^2\ L_T(f)}. \tag{8}$$

Based on (4) and (7), the ratio between $P_{L,\mathrm{TMPP}}$ and P'_L, $\Re$, is

$$\Re = \frac{P_{L,\mathrm{TMPP}}}{{P'}_L} = \frac{1}{2}\left[1 + \sqrt{1 + \left(\frac{k_f\ k_L}{k_R}\ \tan\phi_0\right)^2}\right] \tag{9}$$

where $\tan\ \phi_0 = \frac{2\ \pi\ f_0\ L_T(f_0)}{R_T(T_0)}$, $k_f = \frac{f}{f_0}$ is the ratio between the excitation frequency f and the reference frequency f_0, $k_L = \frac{L_T(f)}{L_T(f_0)}$ is the ratio between the output inductance at the frequency f and that at f_0, and $k_R = \frac{R_T(T)}{R_T(T_0)}$ is the ratio between the output resistance at the operating temperature T and that at T_0.

ϕ_0 defines the characteristic of Z_T at the reference frequency f_0 and reference temperature T_0. $R_T(T_0)$ is the resistance of Z_T at the reference temperature T_0. $L_T(f_0)$ is the inductance of Z_T at the reference frequency f_0. If Z_T is purely resistive, $\phi_0 = 0$. As ϕ_0 increases, Z_T becomes more inductive. If Z_T is purely inductive, $\phi_0\ = 90°$.

Fig. 3 shows the value of $\Re$ versus ϕ_0 with different values of k_f, k_L, and k_R. In general, under low excitation frequency, ϕ_0 is small, $\Re$ is close to unity, and the harvester is operated near the TMPP. As ϕ_0 increases, $\Re$ increases. The operating point of the harvester will deviate from the TMPP.

Furthermore, based on (9), the excitation frequency and operating temperature will affect the value of $\Re$. k_f and k_L give similar effect on $\Re$. As they increase, $\Re$ will increase. Conversely, as k_R increases, $\Re$ will decrease. Fig. 3(a) shows the variation of the $\Re - \phi_0$ curves when k_f or k_L equals 1.2, 1.4, and 1.6, equivalent to an increase of 20%, 40%, and 60%, respectively, in the operating frequency or output inductance. Fig. 3(b) shows the variation of the $\Re - \phi_0$ curves, when k_R equals 1.05, 1.1, and 1.2, equivalent to an increase of 5%, 10%, and 20%, respectively, in the output resistance.

Table I shows the circuit parameters of a commercially available EMEH described in [42]. It also shows the required values of the series-connected resistor R_L and capacitor C_L for matching the output the EMEH. Suggested applications of the harvester are micro wind turbine and hand crank generator. When the excitation frequency is 110 Hz, $\Re = 1.02499$. Then, if the load is a power factor corrector, the extracted power is close to the

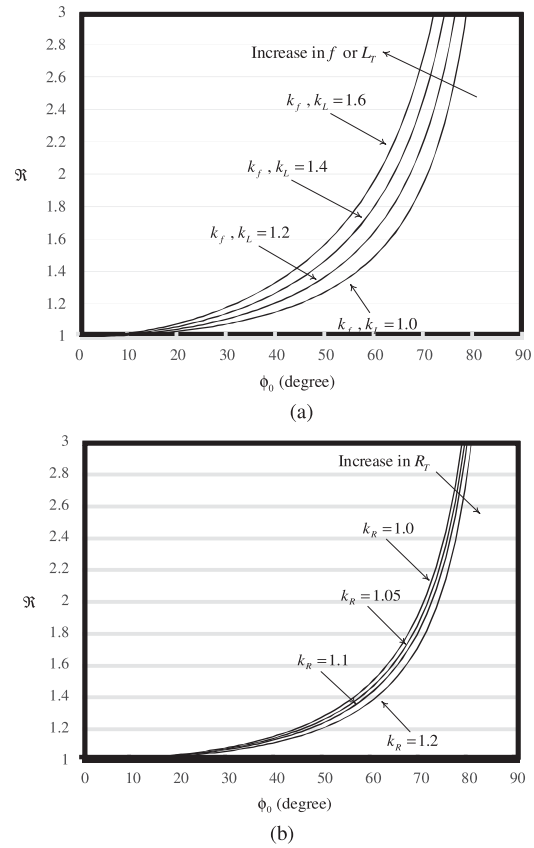

Fig. 3. $\Re$ versus ϕ_0 with different k_f, k_L, and k_R. (a) With $k_R = 1$. (b) With k_f, $k_L = 1$.

TABLE I
PARAMETERS OF A 7-W ELECTROMAGNETIC HARVESTER AND REQUIRED VALUES OF C_L AND R_L

Parameter	Frequency	
	110Hz	170Hz
	Value	Value
v_T * (V)	6.34	9.95
R_T (Ω)	1.28	1.45
L_T (mH)	0.593	0.930
R_L (Ω)	1.28	1.45
C_L (mF)	3.5	1
$\Re$	1.02499	1.106

*Open-circuit voltage when the load is disconnected.

Authorized licensed use limited to: Chulalongkorn University provided by UniNet. Downloaded on August 25,2020 at 06:24:19 UTC from IEEE Xplore. Restrictions apply.

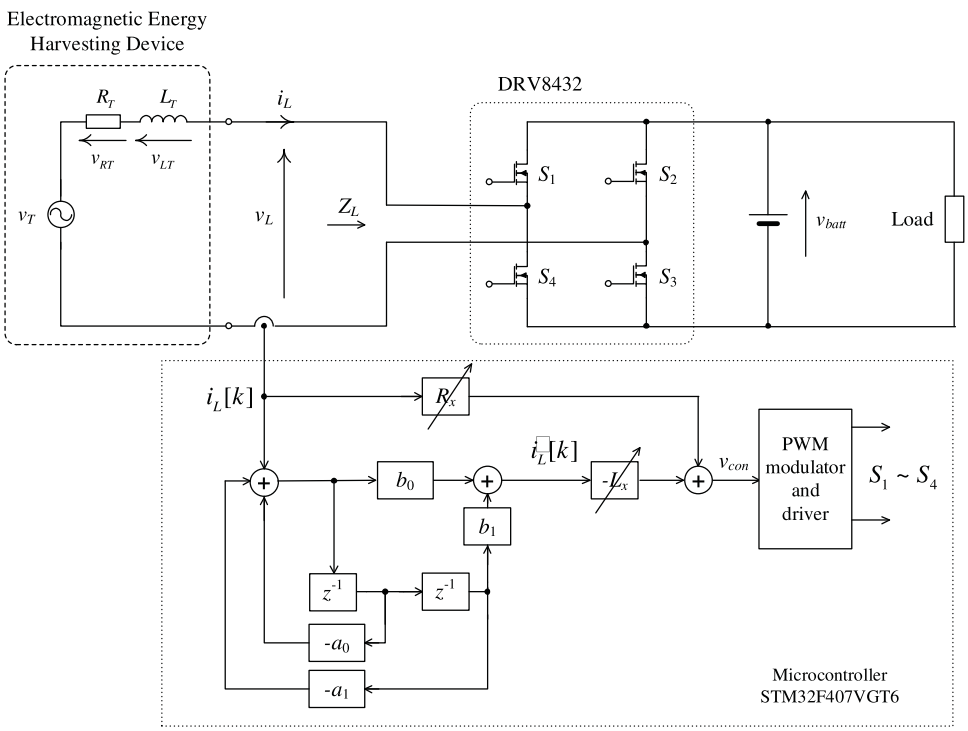

Fig. 4. Proposed MPPT architecture.

maximum extractable power from the harvester. The difference is 2.499%. However, if the excitation frequency is 170 Hz, $\Re = 1.10608$. The power extracted becomes (1.106 – 1)/1.106 = 9.584% less than the maximum extractable power. It is thus crucial to have the load being capacitive to eliminate the effect of the output inductance. The value of the equivalent capacitance C_L should be frequency dependent, as defined in (8). Hence, C_L cannot be implemented by a passive, fixed-value capacitor and should be decreased with the increase in the operating frequency. For example, the required value of C_L at 110 Hz is 3.5 mF and that at 170 Hz is 1 mF. The proposed MPPT aims to control its input impedance to exhibit such operational characteristics.

III. Proposed MPPT Technique

As discussed in Section II, in order to operate the harvester at the TMPP, the load type should be capacitive with the capacitance and load resistance being frequency and temperature dependent. Instead of using passive components, the load is realized by a converter with its input impedance exhibiting the abovementioned load characteristics.

At the TMPP, as shown in Fig. 2(b), the voltage across R_L, v_{RL}, is the same as the voltage across R_T, v_{RT}, that is

$$v_{RL}(T,\ f) = v_{RT}(T,\ f) = R_L\ i_L(T, f) = R_T(T)\ i_L(T,\ f). \tag{10}$$

Moreover, the voltage across C_L, v_{CL}, should be of the same wave shape, but opposite value, as the voltage across L_T, v_{LT}. Thus

$$v_{CL}(T,\ f) = -v_{LT}(T,\ f) = -L_T(f)\ \frac{d\ i_L(T,\ f)}{d\ t}. \tag{11}$$

The load voltage, v_L, equals the algebraic sum of v_{RL} and v_{CL}

$$\begin{aligned} v_L(T,\ f) &= v_{RL}(T,\ f) + v_{CL}(T,\ f) \\ &= R_T(T)\ i_L(T,\ f) - L_T(f)\ \frac{d\ i_L(T,\ f)}{d\ t}. \end{aligned} \tag{12}$$

Thus, the harvester will be operated at the TMPP if v_L is profiled to be the same as the expression given in (12). As shown in Fig. 4, v_L is generated by a bidirectional ac/dc converter with its dc side connected to a rechargeable battery. Some structures require a regulated voltage. Then, an additional dc–dc converter is connected to the output [43]. The power processing circuit of the converter consists of four switching devices, $S_1\ - S_4$. The sensing variable is the load current i_L only. A digital controller is used to generate the gate signals for the switching devices and estimate the values of R_T and L_T under different operating temperatures and excitation frequencies.

As depicted in Fig. 4, R_x and L_x are used to obtain the values of R_T and L_T with (12) as the basis for generating the output voltage of the ac/dc converter. The modulating signal, $v_{\rm con}$, for generating the gate signals for the switching devices is

$$v_{\rm con} = R_x\ i_L(T,\ f) - L_x\ \frac{d\ i_L(T,\ f)}{d\ t}. \tag{13}$$

An EMEH is modeled by a Thevenin's equivalent circuit consisting of an ideal voltage source v_T and an output impedance Z_T [6], [13], [31], [39], [40]. It is shown in Fig. 2. v_T represents the total voltage induced in the coil(s).

The above expression requires differentiating the load current. However, differentiators are generally sensitive to high-frequency noise, due to the sampler, switching noise, stray noise,

Authorized licensed use limited to: Chulalongkorn University provided by UniNet. Downloaded on August 25,2020 at 06:24:19 UTC from IEEE Xplore. Restrictions apply.

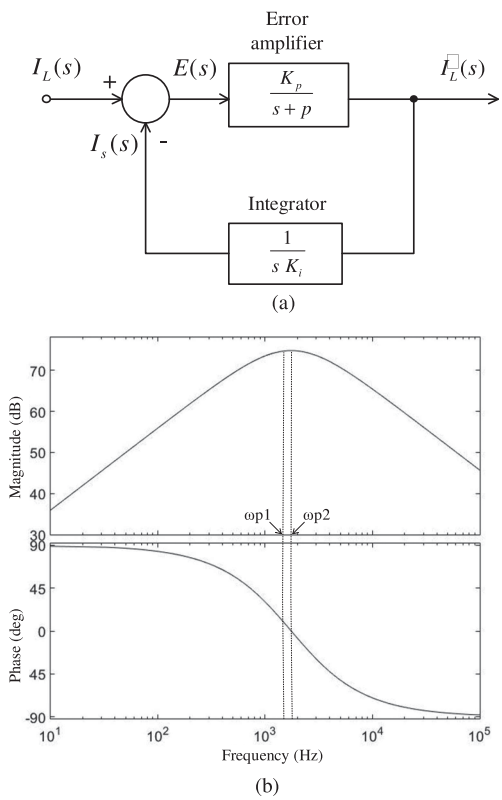

Fig. 5. Differentiator using integrator. (a) Architecture. (b) Frequency characteristic.

crosstalk effect, etc. In order to mitigate the noise problem, the differentiation function is realized by an integrator. As depicted in Fig. 5(a), a feedback loop consisting of an error amplifier and an integrator is used to perform the differentiation. The output of the error amplifier is integrated by an integrator, with the output compared with the actual output current. The error amplifier minimizes the error between the integrated value of its output $I_L(s)$ with the actual input $I_L(s)$. The output of the error amplifier is the differentiated value of the load current, $\dot{I}_L(s)$.

The transfer function of the integrator is

$$\frac{I_s(s)}{\dot{I}_L(s)} = \frac{1}{s\,K_i} \tag{14}$$

where $I_s(s)$ is the output of the integrator and K_i is the time constant of the integrator.

The error amplifier is a simple proportional-plus-integral controller with the transfer function of

$$\frac{\dot{I}_L(s)}{E(s)} = \frac{K_p}{s+p} \tag{15}$$

where $E(s) = I_L(s) - I_s(s)$ is the error between $I_L(s)$ and $I_s(s)$, and K_p and p are the gain and the pole location of the error amplifier, respectively.

By using (14) and (15), the transfer function of the differentiator is

$$\frac{\dot{I}_L(s)}{I_L(s)} = \frac{K_p\,s}{s^2 + p\,s + K_p\,/\,K_i}. \tag{16}$$

The designed transfer characteristic is shown in Fig. 5(b). Equation (16) is rewritten as

$$\frac{\dot{I}_L(s)}{I_L(s)} = \frac{s\,K}{(s+\omega_{P1})\,(s+\omega_{P2})} \tag{17}$$

where $K = K_p$, $\omega_{P1} + \omega_{P2} = p$, and $\omega_c^2 = \omega_{P1}\,\omega_{P2} = K_p\,/\,K_i$.

$-\omega_{P1}$ and $-\omega_{P2}$ are the closed-loop poles of the differentiator, which performs differentiation function for frequency below ω_{P1} and integration function for frequency above ω_{P2}. ω_{P1} is designed to be 10 times higher than the designed excitation frequency, so that the phase of (17) can be maintained around 90° [Fig. 5(b)] and the high-frequency noise can be attenuated.

Equation (17) is realized by the direct form for finite-impulse-response digital filter [44]. By applying bilinear transformation [45], put $s = \frac{2}{T}(\frac{z-1}{z+1})$ and $K_i = 1$, (17) becomes

$$\begin{aligned} F(z) &= \frac{\dot{I}_L(z)}{I_L(z)} \\ &= \frac{{\omega_c}^2\,\left(\frac{2}{T}\,\frac{z-1}{z+1}\right)}{\frac{4}{T^2}\left(\frac{z-1}{z+1}\right)^2 + p\,\left(\frac{2}{T}\,\frac{z-1}{z+1}\right) + \omega_c^2} \end{aligned} \tag{18}$$

where T is the sampling period.

Thus

$$F(z) = \frac{b_0 + b_1\,z^{-2}}{1 + a_0\,z^{-1} + a_1\,z^{-2}} \tag{19}$$

where

$$\begin{aligned} \alpha &= 4 + 2\,p\,T + \omega_c^2\,T^2 \\ a_0 &= \frac{-8 + 2\,\omega_c^2\,T^2}{\alpha} \\ a_1 &= \frac{4 - 2\,p\,T + 2\,\omega_c^2\,T^2}{\alpha}, \quad b_0 = \frac{2\,{\omega_c}^2\,T}{\alpha} \end{aligned}$$

and

$$b_1 = -b_0.$$

The output $\dot{i}_L[k]$ can be expressed as

$$\begin{aligned} \dot{i}_L[k] = {} & b_0\,i_L[k] + b_1\,i_L[k-2] \\ & - a_0\,\dot{i}_L[k-1] - a_1\,\dot{i}_L[k-2]. \end{aligned} \tag{20}$$

Based on (13) and (20), the discrete form of the modulating signal $v_{\rm con}$ for the PWM modulator can be expressed as

$$\begin{aligned} v_{\rm con}[k] = {} & R_x\,i_L[k] - L_x(b_0\,i_L[k] + b_1\,i_L[k-2] \\ & -\,a_0\,\dot{i}_L[k-1] -\,a_1\,\dot{i}_L[k-2]). \end{aligned} \tag{21}$$

The duty cycle of the switching devices S_1 and S_3 is $d[k]$ and that of S_2 and S_4 is $[1 - d[k]]$. $d[k]$ can be expressed as

$$d[k] = \frac{v_{\rm con}[k]}{v_{\rm Batt}[k]} \tag{22}$$

where $v_{\rm Batt}$ is the battery voltage.

Authorized licensed use limited to: Chulalongkorn University provided by UniNet. Downloaded on August 25,2020 at 06:24:19 UTC from IEEE Xplore. Restrictions apply.

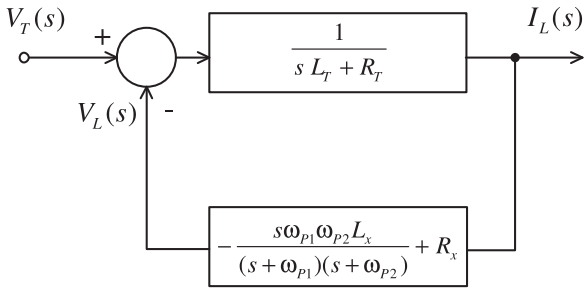

Fig. 6. Block diagram of the overall system.

IV. System Modeling

As shown in Fig. 4, the load current i_L can be expressed as

$$I_L(s) = \frac{V_T(s) - V_L(s)}{s\,L_T + R_T}. \tag{23}$$

Based on (13) and (17), with $K_i = 1$

$$\begin{aligned} V_L(s) &= -L_x\,\dot{I}_L(s) + R_x\,I_L(s) \\ &= \left(-\frac{s\,\omega_{P1}\,\omega_{P2}\,L_x}{(s+\omega_{P1})\,(s+\omega_{P2})} + R_x\right)\,I_L(s). \end{aligned} \tag{24}$$

By using (23) and (24), the equivalent output impedance, Z_{out}, on v_T is

$$\begin{aligned} Z_{\text{out}}(s) &= \frac{V_T(s)}{I_L(s)} \\ &= s\,L_T - \frac{s\,\omega_{P1}\,\omega_{P2}\,L_x}{(s+\omega_{P1})\,(s+\omega_{P2})} + (R_T + R_x). \end{aligned} \tag{25}$$

Hence, v_T and i_L are in phase when

$$L_x = \frac{(\omega_{P1}\,\omega_{P2} - \omega^2)^2 + (\omega_{P1} + \omega_{P2})^2\,\omega^2}{\omega_{P1}\,\omega_{P2}\,(\omega_{P1}\,\omega_{P2} - \omega^2)}\,L_T. \tag{26}$$

The harvester will be operated at the TMPP when $\text{Re}[Z_{\text{out}}(j\omega)] = 2\,R_T$. Based on (25)

$$R_x = R_T + \frac{(\omega_{P1} + \omega_{P2})\,\omega^2}{\omega_{P1}\,\omega_{P2} - \omega^2}\,L_T. \tag{27}$$

If $\omega << \omega_{P1}$ and ω_{P2}, $L_x = L_T$ and $R_x = R_T$.

Fig. 6 shows the block diagram of the system. $I_L(s)$ is expressed as (28) shown at the bottom of this page.

The characteristic equation of $I_L(s)$ is a cubic function. As the coefficient of s^3 term is very small, the characteristic equation can be simplified into a second-order function $Q(s)$

$$\begin{aligned} Q(s) = &\frac{(\omega_{P1} + \omega_{P2})L_T + (R_T + R_x)}{\omega_{P1}\,\omega_{P2}}\,s^2 \\ &+ \left[\frac{(\omega_{P1} + \omega_{P2})(R_T + R_x)}{\omega_{P1}\,\omega_{P2}} + (L_T - L_x)\right]\,s \\ &+ (R_T + R_x). \end{aligned} \tag{29}$$

It can be approximated that the root of $Q(s)$ will be on the left half s-plane when

$$L_x < L_{x,\text{crit}} \tag{30}$$

where $L_{x,\text{crit}} = L_T + \frac{\omega_{P1}+\omega_{P2}}{\omega_{P1}\,\omega_{P2}}\,(R_T + R_x)$.

Thus, the system is stable when (30) is satisfied. Conversely, the system becomes unstable. Based on this property, the value of L_T is determined by observing the change of the current waveform with the value of L_x

$$L_T = L_{x,\text{crit}} - \frac{\omega_{P1} + \omega_{P2}}{\omega_{P1}\,\omega_{P2}}\,(R_T + R_x). \tag{31}$$

If ω_{P1} and ω_{P2} are large, $L_T = L_{x,\text{crit}}$.

The value of R_T is determined by observing the change of the extracted power with the value of R_x.

V. Procedure of Determining the Values of L_T and R_T

The values of L_T and R_T are determined in two steps. The first one is to determine the value of L_T and the second one is to determine R_T. L_T is determined by perturbing the value of L_x on the controller. Based on (30), the system becomes unstable when $L_x > L_{x,\text{crit}}$. The amplitude of the current waveform will increase until a saturation nonlinearity in the system appears. The current waveform will then be distorted. The crest factor of i_L, CF, is used to determine whether L_x has reached the value of $L_{x,\text{crit}}$. It is defined as the ratio between the peak value, $I_L|_{\text{PEAK}}$, and the rms value, $I_L|_{\text{rms}}$, of i_L,

$$\text{CF} = \frac{I_L|_{\text{PEAK}}}{I_L|_{\text{rms}}}. \tag{32}$$

The values of $I_L|_{\text{PEAK}}$ and $I_L|_{\text{rms}}$ are determined by

$$I_L|_{\text{PEAK}} = \frac{1}{2}\,(I_{L,\max} + I_{L,\min}) \tag{33}$$

$$I_L|_{\text{rms}} = \sqrt{\frac{1}{N_s}\,\sum\nolimits_{k=1}^{N_s}\,(i_L[k])^2} \tag{34}$$

where $I_{L,\max}$ and $I_{L,\min}$ are the maximum and minimum values of i_L over the data length N_s.

Fig. 7 shows the measured CF versus L_x of the prototype that will be discussed in Section VI. The excitation frequency is 170 Hz. If the excitation is sinusoidal, the value of CF is ideally equal to 1.414 under stable operation. When L_x is increased to $L_{x,\text{crit}}$ (1.45 mH), the value of CF is increased suddenly, confirming the property of the system stability discussed above. Hence, $L_{x,\text{crit}}$ is taken as the threshold for estimating the value of L_T.

Fig. 8 shows the flowchart for determining the value of L_T. The value of L_x starts with the minimum value $L_{x,\min}$, that is, $L_x[0] = L_{x,\min}$ and $R_x = 0$. Practically, the initial value of R_x can be set higher in order to reduce inrush current. Then, L_x is increased progressively in step of ΔL_x, if CF is within the range

$$I_L(s) = \frac{(s+\omega_{P1})(s+\omega_{P2})}{(s+\omega_{P1})(s+\omega_{P2})(s\,L_T + R_T + R_x) - s\,\omega_{P1}\,\omega_{P2}\,L_x}\,V_T(s) \tag{28}$$

Authorized licensed use limited to: Chulalongkorn University provided by UniNet. Downloaded on August 25,2020 at 06:24:19 UTC from IEEE Xplore. Restrictions apply.

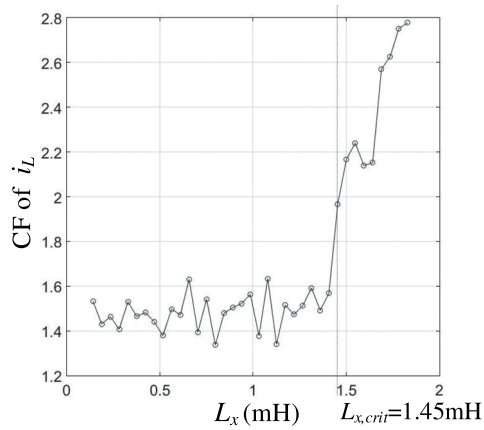

Fig. 7. Measured crest factor of i_L versus L_x with $R_x = 0$.

of 1.414 ± 20%, where i_L is sinusoidal, that is

$$L_x[n+1] = L_x[n] + \Delta L_x. \tag{35}$$

Conversely, if CF is outside the above range, L_x will be changed back to its previous value. The final value of L_x is treated as the value of L_T by using (31) as

$$L_T \approx L_x[n] - \Delta L_x - \frac{\omega_{P1} + \omega_{P2}}{\omega_{P1}\,\omega_{P2}}\, R_{T,p} \tag{36}$$

where $R_{T,p}$ is the value of R_T obtained in previous cycle of determining the value of R_x.

The value of R_T is determined by perturbing the value of R_x and observing the change of the power extracted. The extracted power, p_L, is obtained indirectly by using the sampled value of i_L and $R_x[j]$, that is

$$p_L[k] = (i_L[k])^2\, R_x[j]. \tag{37}$$

The average value of p_L, P_L, is

$$P_L = \frac{1}{N_s}\sum_{k=1}^{N_s} p_L[k]. \tag{38}$$

If P_L increases with the increase in the value of R_x, R_x will be increased by ΔR_x

$$R_x[j+1] = R_x[j] + \Delta R_x. \tag{39}$$

Otherwise

$$R_x[j+1] = R_x[j] - \Delta R_x. \tag{40}$$

If P_L increases with the decrease in R_x, R_x will be decreased by ΔR_x, that is

$$R_x[j+1] = R_x[j] - \Delta R_x. \tag{41}$$

Otherwise

$$R_x[j+1] = R_x[j] + \Delta R_x. \tag{42}$$

If the absolute difference between $P_L[j+1]$ and $P_L[j]$ is smaller than a tolerance ε_P, that is

$$|P_L[j+1] - P_L[j]| < \varepsilon_P \tag{43}$$

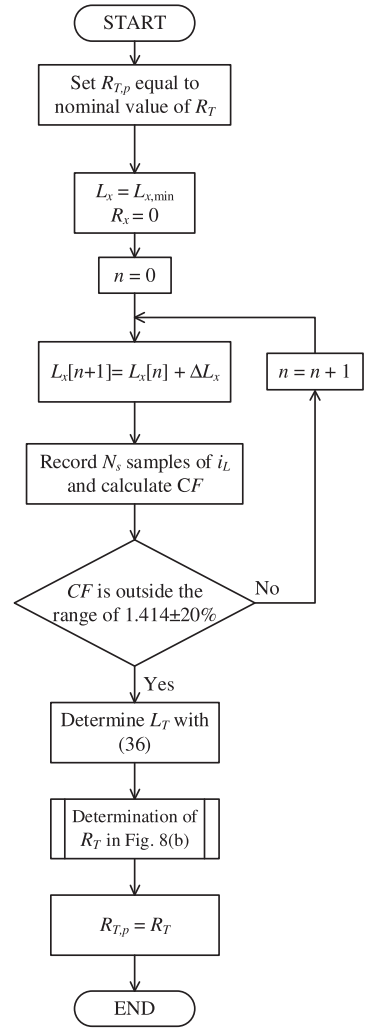

Fig. 8. Flowchart of the algorithm. (a) Determination of L_T and R_T. (b) Subprocess for determining R_T.

Authorized licensed use limited to: Chulalongkorn University provided by UniNet. Downloaded on August 25,2020 at 06:24:19 UTC from IEEE Xplore. Restrictions apply.

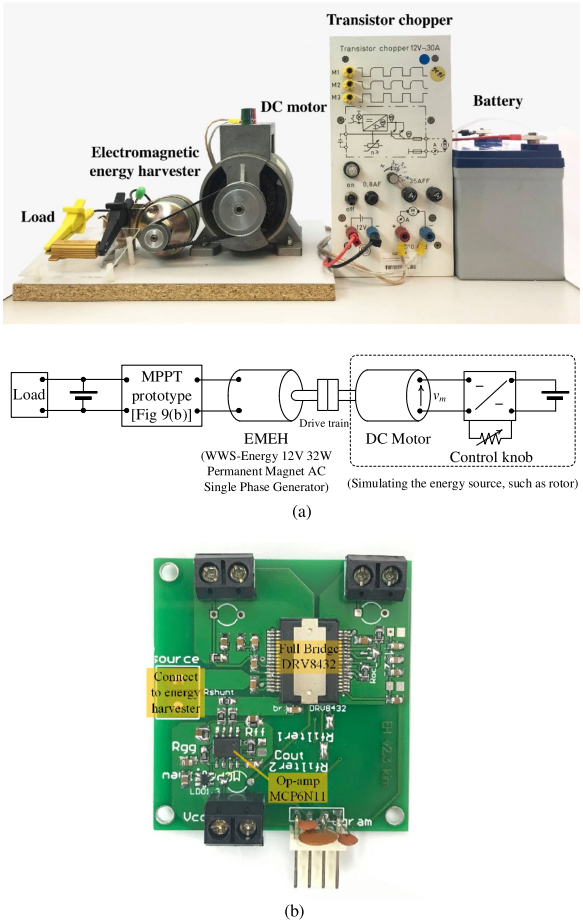

Fig. 9. Experimental setup. (a) Setup for testing the output characteristics of the harvester. (b) MPPT prototype.

the above P&O procedure will be terminated.

Based on (27) and (31)

$$R_T \approx \left[1 - \frac{\omega^2 \left(\omega_{P1} + \omega_{P2}\right)^2}{\omega_{P1}\omega_{P2}(\omega_{P1}\omega_{P2} - \omega^2)}\right]^{-1} \times \left[R_x[j] - \frac{\omega^2 \left(\omega_{P1} + \omega_{P2}\right)}{\omega_{P1}\omega_{P2} - \omega^2} L_{x,\text{crit}}\right]. \quad (44)$$

If $\omega_{P1}, \omega_{P2} \gg \omega$, $R_T = R_x[j]$.

Such P&O procedures are repeatedly executed to determine the values of L_T and R_T. It has several merits. First, it requires sensing the output current of the harvester only. Second, it can locate the TMPP of the harvester without requiring *a priori* knowledge of R_T and L_T under different operating conditions, such as temperature, excitation frequency, and change of L_T with excitation frequency. Third, the algorithm is software based without increasing the circuit complexity, as compared to some techniques using H-bridge circuit as the power processing circuit [32]–[37].

VI. Experimental Verifications

A prototype for locating the TMPP of a 7-W electromagnetic harvester has been built and evaluated. Fig. 9(a) shows the setup for testing the output characteristic of the harvester. The harvester is driven by a dc motor and the speed of rotation is controlled by a transistor chopper, which can adjust the terminal voltage V_M applied to the motor. Table I shows the characteristics under the excitation frequency of 110 and 170 Hz, respectively. Fig. 9(b) shows the prototype for extracting the TMPP of the harvester. The dc motor is used to simulate the energy source to drive the EMEH (i.e., single-phase PM generator), like the rotor in a wind-turbine system. The output of the EMEH is connected to different load types and values, so that the output resistance and output inductance under different operating conditions are determined. The MPPT prototype, shown in Fig. 9(b), is designed to connect to the output of the EMEH. The mechanical energy source can be converted into electrical energy by many methods, such as driven with rotor in wind turbine system, continuously variable transmission in [3], and rack and pinion system in [4], [7], [8], [31]–[33].

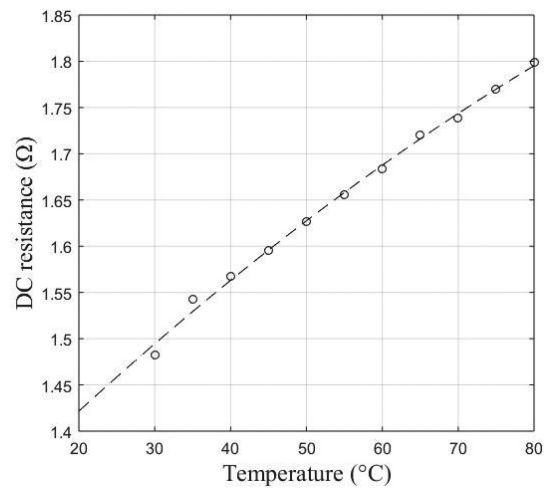

Fig. 10. Measured dc resistance of the inductor.

For the sake of analysis and investigation, the harvester is modeled by an ac voltage source with a series inductor [6], [13], [31], [39], [40]. The inductance of the inductor is 0.938 mH. The excitation frequency is 170 Hz. The resistance of the inductor varies with the temperature. Fig. 10 shows the measured dc resistance of the inductor at different temperatures. The resistance increases by more than 20%, when the operating temperature is increased from 30 °C to 80 °C. Thus, the maximum extractable power and operating point of the harvester are affected by the operating temperature.

The controller of the MPPT is STM32F407VGT6 and the full-bridge module is Texas Instruments DRV8432. The switching frequency is 100 kHz and the sampling frequency of the terminal voltage and current is 12.5 kHz. The control parameters are tabulated in Table II. The total power consumption of the drivers and microcontroller is found to be 0.537 W.

Figs. 11 and 12(a)–(d) show the measurement results with the proposed MPPT connected to the source. Fig. 11 shows the waveforms of i_L. The P&O procedure, as depicted in Section V, is divided into two stages, including Stage 1 and Stage 2. The value of L_T is determined in Stage 1, while the value of R_T is

Authorized licensed use limited to: Chulalongkorn University provided by UniNet. Downloaded on August 25,2020 at 06:24:19 UTC from IEEE Xplore. Restrictions apply.

TABLE II
VALUES OF THE PARAMETERS USED IN THE PROTOTYPE

Parameter	Value	Parameter	Value
a_0	-0.77841552	p	21991
a_1	0.15127693	T	$8\,e^{-5}$
b_0	2331.1872	ω_c	10991
b_1	-2331.1872	ω_{p1}	2π 1700
K	120803957	ω_{p2}	2π 1800

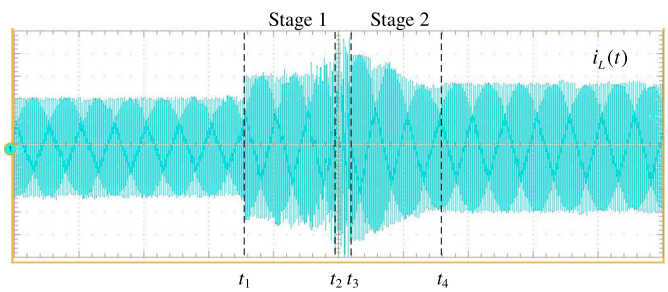

Fig. 11. Measured waveform of i_L throughout the perturb-and-observe process. $i_L(t)$:1 A/ div. Timebase: 200 ms/div.

determined in Stage 2. The procedure is based on the flowchart given in Fig. 8. The operation of each stage is described as follows.

A. Stage 1—Determination of L_T

This stage starts at t_1 and ends at t_3. The inductance L_x is increased from zero in step of 5% of the nominal value of L_T between t_1 and t_2. At t_2, i_L becomes nonsinusoidal. Then, the value of L_x is reduced back to the previous one at t_3. The value of L_x is chosen to be $L_{x,\text{crit}}$ for calculating the value of L_T with (31). Fig. 12(a)–(c) shows the detailed waveforms of v_T and i_L between t_1 and t_2, between t_2 and t_3, and after t_3, respectively.

B. Stage 2—Determination of R_T

After determining the value of L_T, R_T is determined by considering the power extracted from the harvester. The instantaneous and average power extracted are determined by (37) and (38), respectively. R_x will be increased or decreased based on the change of the average power extracted. The mechanism is based on the P&O algorithm shown in Fig. 8(b).

The time span between t_2 and t_3 is 50 ms. The whole process lasts 0.57 s. Fig. 12(d) shows the waveforms of v_T and i_L after the entire P&O process. The two waveforms are in phase, confirming that the proposed MPPT can eliminate the effect of the output inductance.

For the sake of comparison, Fig. 12(e) shows the measurement results with pure resistive load connected to the source. The two waveforms are not in phase. The waveforms of v_T in Fig. 12 contain high-frequency ripple. It is mainly due to the

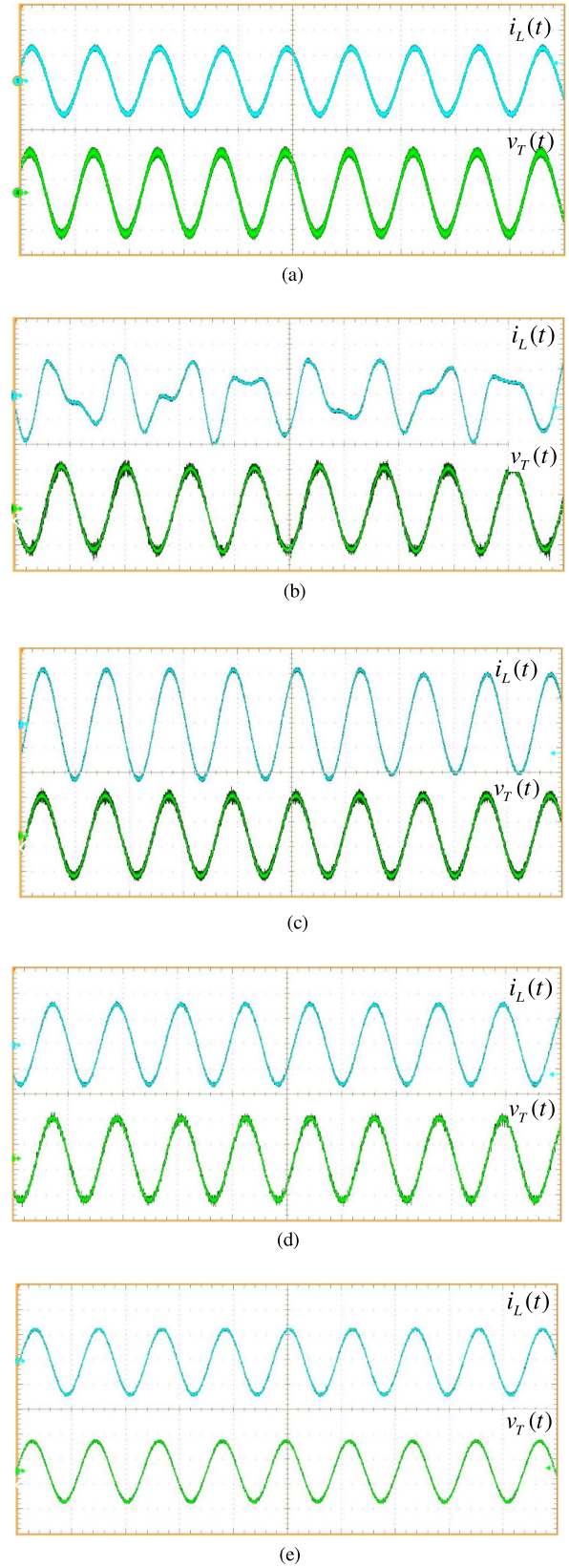

Fig. 12. Measured waveforms of i_L and $v_T(t)$. (a) At the beginning of Stage 1. $i_L(t)$: 2 A/ div. $v_T(t)$: 6 V/ div. Timebase: 5.0 ms/ div. (b). Between t_2 to t_3. $i_L(t)$: 5 A/ div. $v_T(t)$: 6 V/ div. Timebase: 5.0 ms/ div. (c) At the beginning of Stage 2. $i_L(t)$: 2 A/ div. $v_T(t)$: 6 V/div. Timebase: 5.0 ms/ div. (d) At the end of Stage 2. $i_L(t)$: 2 A/ div. $v_T(t)$: 6 V/ div. Timebase: 5.0 ms/ div. (e) With pure resistive load. $i_L(t)$: 2 A/ div. $v_T(t)$: 8 V/ div. Timebase: 5.0 ms/ div.

Authorized licensed use limited to: Chulalongkorn University provided by UniNet. Downloaded on August 25,2020 at 06:24:19 UTC from IEEE Xplore. Restrictions apply.

presence of the output impedance of the ac voltage source. The output impedance varies with frequency. At 170 Hz, the output impedance is found to be 9 mΩ. At high frequency, the output impedance is 4 Ω, where the high-frequency current ripple of 316 mA causes a ripple voltage of 1.26 V.

Fig. 13(a)–(d) shows the measurement results with the proposed MPPT and pure resistive load, respectively. They show the extracted power versus the values of R_L' [Fig. 1(a)] and R_L [Fig. 1(b)], which is implemented on the controller with the above control algorithm under different operating conditions. With the operating temperature at 40 °C and excitation frequency of 170 Hz, Fig. 13(a) shows that the power extracted with the proposed MPPT is 7.158 W and that with pure resistor is 6.762 W. Thus, there is a 5.86% power increment with the proposed MPPT.

With the operating temperature at 24 °C and excitation frequency of 170 Hz, Fig. 13(b) shows that the power extracted with the proposed MPPT is 7.956 W and that with pure resistor is 7.22 W. Thus, there is a 10.2% power increment with the proposed MPPT.

With the operating temperature at 40 °C and excitation frequency of 110 Hz, Fig. 13(c) shows that the power extracted with the proposed MPPT is 7.485 W and that with pure resistor is 7.222 W. Thus, there is a 3.64% power increment with the proposed MPPT.

With the operating temperature at 24 °C and excitation frequency of 110 Hz, Fig. 13(d) shows that the power extracted with the proposed MPPT is 7.96 W and that with pure resistor is 7.71 W. Thus, there is a 3.24% power increment with the proposed MPPT.

It should be noted that there is only one matched condition in each case. There is only one value of R_L' or R_L in the respective case that can extract the power maximally from the harvester (Fig. 2), at which the input impedance of the MPPT is matched with the output impedance of the harvester.

Thus, the discrepancy between the power extracted by a pure resistor and the maximum extractable power from the harvester increases as the excitation frequency increases and operating temperature reduces, confirming with the discussions in Section II.

It can be seen from the above procedure and test that the proposed MPPT can automatically determine the values of L_T and R_T, so as to operate the harvester at the TMPP. It should be noted that the approach of determining the values is conservative. Further research can be dedicated to accelerate the determination process and investigate the behaviors under non-sinusoidal excitation. Nevertheless, locating the unstable point for determining the value of L_T and locating the MPP for determining the value of R_T are the basic principle in the entire estimation.

Fig. 14(a) shows the measured waveforms when the source is subject to a low-frequency perturbation. The proposed MPPT algorithm starts at t_A and ends at t_B. It totally takes 470 ms to finish the whole process. Fig. 14(b) shows the current and voltage waveforms before the proposed MPPT algorithm is activated. The current i_L is not in phase with the voltage v_T. Fig. 14(c) shows the current and voltage waveforms before the proposed

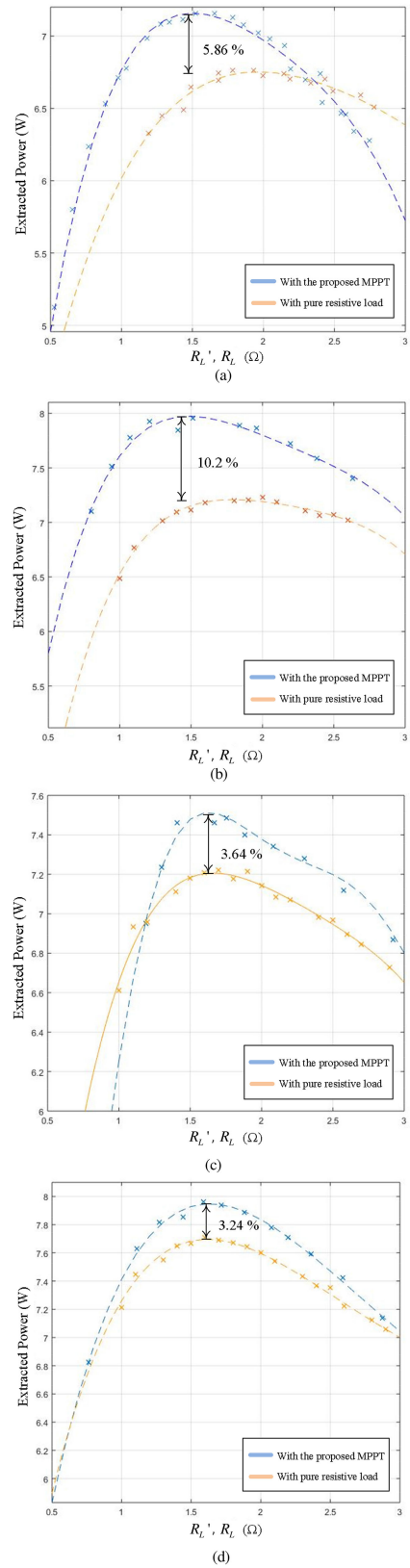

Fig. 13. Power extracted versus R_L' in Fig. 1(a) and R_L in Fig. 1(b) under different operating conditions. (a) Temperature = 40 °C and frequency = 170 Hz. (b) Temperature = 24 °C and frequency = 170 Hz. (c) Temperature = 40 °C and frequency = 110 Hz. (d) Temperature = 24 °C and frequency = 110 Hz.

Authorized licensed use limited to: Chulalongkorn University provided by UniNet. Downloaded on August 25,2020 at 06:24:19 UTC from IEEE Xplore. Restrictions apply.

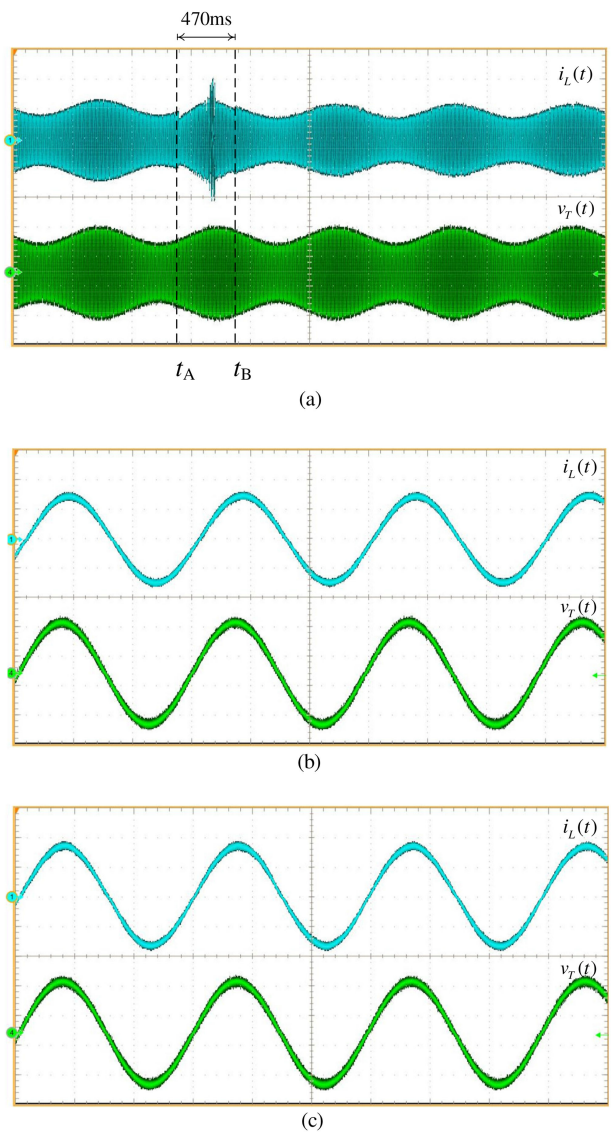

Fig. 14. Measured voltage and current waveforms when the harvester output is subject to a low-frequency variation. (a) Overall profile (i_L: 3 A/div, v_T: 6 V/div, Timebase: 500 ms/s). (b) Before performing the proposed MPPT (i_L: 2 A/div, v_T: 5 V/div, Timebase: 2 ms/s). (c) After performing the proposed MPPT (i_L: 2 A/div, v_T: 5 V/div, Timebase: 2 ms/s).

MPPT algorithm is activated. The current i_L is in phase with the voltage v_T. The test confirms that the proposed MPPT algorithm can track the MPP of the harvester. Nevertheless, further research will be dedicated to exploring ways to shorten the time taken for tracking the MPP.

VII. Conclusion

An MPPT that can operate an EMEH at the TMPP has been presented. Its power conversion stage is a bidirectional ac/dc converter. It is controlled to cancel the effect of the output inductance and then match the output resistance of the harvester, so that the power extracted from the harvester is maximized. The TMPP is located by observing the change of the crest factor of the output current of the harvester with respect to the change of the assumed value of the output inductance and also observing the variation of the extracted power with respect to the change of the assumed value of the output resistance of the harvester on the controller. The proposed technique has been verified on a 7-W prototype. Results find that the power extracted by the proposed MPPT is higher than that extracted by a pure resistive load, confirming the merit of the proposed MPP tracking technique as compared to prior art.

In terms of the hardware configuration, the proposed circuit is similar to or simpler than prior art [32]–[36] that create a complex impedance with an H-bridge as the power conversion stage on the output of the EMEH. Compared with [32], [33], the proposed system does not require a tachometer to measure the speed of rotation to calculate the current demand. Compared with [34], the system architecture is basically the same. An application-specific integrated power converter was proposed in [34], while commercially available integrated circuits are utilized in the system to demonstrate the proposed MPPT technique. The controller used in [35] is dSPACE DS1104 development microcontroller system which is more complex than the proposed method. In [36], as shown in Fig. 4-3, the controller is implemented with analog circuit.

With similar hardware configuration, the major difference between the proposed method and prior art is control objectives. Prior art creates conjugate impedance to match with the output impedance of the EMEH with the coil parameters known *a priori*, while the proposed method does not require knowing the coil parameters. The controller determines the coil parameters via a P&O algorithm.

References

[1] S. Wang, Y. Ke, P. Huang, and P. Hsieh, "Electromagnetic energy harvester interface design for wearable applications," *IEEE Trans. Circuits Syst. II*, vol. 65, no. 5, pp. 667–671, May 2018.

[2] L. Rome, L. Flynn, and E. Goldman, "Generating electricity while walking with loads," *Science*, vol. 309, pp. 1725–1728, Sep. 2005.

[3] Y. Ikawa, T. Kobayashi, and T. Matsubara, "Biomechanical energy harvester with continuous variable transmission: Prototyping and preliminary evaluation," in *Proc. IEEE/ASME Int. Conf. Adv. Intell. Mechatron.*, Sep. 2018, pp. 1045–1050.

[4] M. Abdelkareem *et al.*, "Vibration energy harvesting in automotive suspension system: A detailed review," *Appl. Energy*, vol. 229, pp. 672–699, Nov. 2018.

[5] M. Trapanese, "Optimization of a sea wave energy harvesting electromagnetic device," *IEEE Trans. Magn.*, vol. 44, no. 11, pp. 4365–4368, Nov. 2008.

[6] P. Spies, L. Mateu, and M. Pollak, *Handbook of Energy Harvesting Power Supplies and Application*. Singapore: Pan Stanford Publishing, 2015.

[7] D. Dinulovic, M. Brooks, M. Haug, and T. Petrovic, "Rotational electromagnetic energy harvesting system," *Phys. Procedia*, vol. 75, pp. 1244–1251, 2015.

[8] J. Siang, M. Lim, and M. S. Leong, "Review of vibration-based energy harvesting technology: Mechanism and architectural approach," *Int. J. Energy Res.*, vol. 42, no. 5, pp. 1866–1893, Apr. 2018.

[9] D. Spreemann and Y. Manoli, *Electromagnetic Vibration Energy Harvesting Devices: Architectures, Design, Modeling and Optimization*. New York, NY, USA: Springer, 2012.

[10] G. Szarka, P. Proynov, B. Stark, S. Burrow, and N. McNeill, "Experimental investigation of inductorless, single-stage boost rectification for sub-mW electromagnetic energy harvesters," in *Proc. IEEE/ACM Int. Symp. Low Power Electron. Des.*, 2011, pp. 361–366.

[11] M. Balato, L. Costanzo, and M. Vitelli, "Resonant electromagnetic vibration harvesters: Determination of the equivalent electric circuit parameters and simplified closed-form analysis for the identification of the optimal diode bridge rectifier DC load," *Int. J. Elect. Power Energy Syst.*, vol. 84, pp. 111–123, 2017.

Authorized licensed use limited to: Chulalongkorn University provided by UniNet. Downloaded on August 25,2020 at 06:24:19 UTC from IEEE Xplore. Restrictions apply.

[12] M. Balato, L. Costanzo, and M. Vitelli, "Maximization of the extracted power in resonant electromagnetic vibration harvesters applications employing bridge rectifiers," *Sensors Actuators A: Phys.*, vol. 263, pp. 63–75, Aug. 2017.

[13] R. Amirtharajah and A. Chandrakasan, "Self-powered signal processing using vibration-based power generation," *IEEE J. Solid-State Circuits*, vol. 33, no. 5, pp. 687–695, May 1998.

[14] L. Costanzo and M. Vitelli, "Resonant electromagnetic vibration harvesters applications: Optimization of P&O MPPT technique parameters," in *Proc. 13th Int. Conf. Ecol. Veh. Renew. Energies*, 2018, pp. 1–8.

[15] M. Balato, L. Costanzo, and M. Vitelli, "MPPT in wireless sensor nodes supply systems based on electromagnetic vibration harvesters for freight wagons applications," *IEEE Trans. Ind. Electron.*, vol. 64, no. 5, pp. 3576–3586, May 2017.

[16] T. O'Connor, J. Hyun, and D. Ha, "Power management circuit for kinetic energy harvesting from freight railcars," in *Proc. IEEE 60th Int. Midwest Symp. Circuits Syst.*, 2017, pp. 1426–1429.

[17] H. Luan, O. Onar, and A. Khaligh, "Dynamic modeling and optimum load control of a PM linear generator for ocean wave energy harvesting application," in *Proc. IEEE Appl. Power Electron. Conf. Expo.*, 2009, pp. 739–743.

[18] P. Mitcheson, T. Green, and E. Yeatman, "Power processing circuits for electromagnetic, electrostatic and piezoelectric inertial energy scavengers," *Microsyst. Technol.*, vol. 13, no. 11–12, pp. 1629–1635, Jul. 2007.

[19] M. Shousha, D. Dinulovic, and M. Haug, "A universal topology based on buck-boost converter with optimal resistive impedance tracking for energy harvesters in battery powered applications," in *Proc. IEEE Appl. Power Electron. Conf. Expo.*, 2017, pp. 2111–2115.

[20] S. Dwari and L. Parsa, "An efficient AC-DC step-up converter for low-voltage energy harvesting," *IEEE Trans. Power Electron.*, vol. 25, no. 8, pp. 2188–2199, Aug. 2010.

[21] H. Wang, Y. Tang, and A. Khaligh, "A bridgeless boost rectifier for low-voltage energy harvesting applications," *IEEE Trans. Power Electron.*, vol. 28, no. 11, pp. 5206–5214, Nov. 2013.

[22] R. Dayal, S. Dwari, and L. Parsa, "A new design for vibration-based electromagnetic energy harvesting systems using coil inductance of microgenerator," *IEEE Trans. Ind. Appl.*, vol. 47, no. 2, pp. 820–830, Mar./Apr. 2011.

[23] Q. Sun, S. Patil, N. Sun, and B. Lehman, "Phase/RMS maximum power point tracking for inductive energy harvesting system," in *Proc. IEEE Energy Convers. Congr. Expo.*, 2015, pp. 408–413.

[24] L. Yu, H. Wang, and A. Khaligh, "A discontinuous conduction mode single-stage step-up rectifier for low-voltage energy harvesting applications," *IEEE Trans. Power Electron.*, vol. 32, no. 8, pp. 6161–6169, Aug. 2017.

[25] Y. Xu, D. Ha, and M. Xu, "Energy harvesting circuit with input matching in boundary conduction mode for electromagnetic generators," in *Proc. IEEE Int. Symp. Circuits Syst.*, 2017, pp. 1–4.

[26] M. Shousha, D. Dinulovic, M. Brooks, and M. Haug, "A miniaturized cost effective shared inductor based energy management system for ultra-low-voltage electromagnetic energy harvesters in battery powered applications," in *Proc. IEEE Appl. Power Electron. Conf. Expo.*, 2018, pp. 703–707.

[27] R. Dayal, K. Modepalli, and L. Parsa, "A new optimum power control scheme for low-power energy harvesting systems," *IEEE Trans. Ind. Appl.*, vol. 49, no. 6, pp. 2651–2661, Nov./Dec. 2013.

[28] G. Szarka, S. Burrow, P. Proynov, and B. Stark, "Maximum power transfer tracking for ultralow-power electromagnetic energy harvesters," *IEEE Trans. Power Electron.*, vol. 29, no. 1, pp. 201–212, Jan. 2014.

[29] Q. Sun, S. Patil, S. Stoute, N. Sun, and B. Lehman, "Optimum design of magnetic inductive energy harvester and its AC-DC converter," in *Proc. IEEE Energy Convers. Congr. Expo.*, 2012, pp. 394–400.

[30] Y. Tang and A. Khaligh, "A multiinput bridgeless resonant AC-DC converter for electromagnetic energy harvesting," *IEEE Trans. Power Electron.*, vol. 31, no. 3, pp. 2254–2263, Mar. 2016.

[31] Q. Sun, S. Patil, N. Sun, and B. Lehman, "Inductive magnetic harvester with resonant capacitive rectifier based on synchronized switch harvesting technique," in *Proc. IEEE Energy Convers. Congr. Expo.*, 2013, pp. 4940–4947.

[32] P. Mitcheson, T. Toh, K. Wong, S. Burrow, and A. Holmes, "Tuning the resonant frequency and damping of an electromagnetic energy harvester using power electronics," *IEEE Trans. Circuits Syst. II*, vol. 58, no. 12, pp. 792–796, Dec. 2011.

[33] N. Kaphengst, T. Toh, P. Mitcheson, A. Holmes, S. Wright, and E. Yeatman, "Adaptive load synthesis for autonomous resonant frequency tuning of electromagnetic energy harvesters," in *Proc. PowerMEMS*, Atlanta, USA, Dec. 2012, pp. 420–423.

[34] U. Radhakrishna *et al.*, "A low-power integrated power converter for an electromagnetic vibration energy harvester with 150 mV-AC cold startup, frequency tuning, and 50 Hz AC-to-DC conversion," in *Proc. IEEE Custom Integr. Circuits Conf.*, 2018, pp. 1–4.

[35] J. Bowden, S. Burrow, A. Cammarano, L. Clare, and P. Mitcheson, "Switched-mode load impedance synthesis to parametrically tune electromagnetic vibration energy harvesters," *IEEE Trans. Mechatron.*, vol. 20, no. 2, pp. 603–610, Apr. 2015.

[36] S. Chang, "Harvesting energy from non-ideal vibrations," Ph.D. thesis, Massachusetts Inst. Technol., Cambridge, MA, USA, 2013. Available: https://dspace.mit.edu/handle/1721.1/82346

[37] K. Tse and H. Chung, "Maximum power point tracker for electromagnetic energy harvesting system," in *Proc. IEEE Energy Convers. Congr. Expo.*, 2017, pp. 5515–5522.

[38] S. Heo, Y. Yang, J. Lee, S. Lee, and J. Kim, "Micro energy management for energy harvesting at maximum power point," in *Proc. Int. Symp. Integr. Circuits*, 2011, pp. 136–139.

[39] W. Choi, H. Kim, C. Park, and B. Lee, "Study on electromagnetic energy transducer in ambient vibration," *IET Power Electron.*, vol. 11, no. 12, pp. 1983–1990, Oct. 2018.

[40] P. Mitcheson, T. Green, E. Yeatman, and A. Holmes, "Architectures for vibration-driven micropower generators," *IEEE J. Microelectromech. Syst.*, vol. 13, no. 3, pp. 429–440, Jun. 2004.

[41] J. Shepherd, A. Morton, and L. Spence, *Higher Electrical Engineering*. Beijing, China: Bitman Books Limited, 2015.

[42] WWS-Energy 12 V 32 W Permanent Magnet AC Single Phase Generator, 2019. [Online]. Available: https://www.aliexpress.com/item/32873421446.html

[43] M. Shousha, D. Dinulovic, M. Haug, and A. Mahgoub, "A bias supply scheme for a self-powered EMS for battery-less IoT applications powered by electromagnetic energy harvesters," in *Proc. 20th Eur. Conf. Power Electron. Appl.*, Riga, Latvia, 2018, pp. 1–6.

[44] C. Phillips and H. Nagle, *Digital Control System Analysis and Design*. Englewood Cliffs, NJ, USA: Prentice-Hall, 1970.

[45] A. Oppenheim and R. Schafer, *Discrete Time Signal Processing*, 3rd ed. Upper Saddle River, NJ, USA: Pearson Higher Education, 2010.

Kimberley Hiu-kwan Tse (Student Member, IEEE) received the B.Eng. degree in electronic and communication engineering from the City University of Hong Kong, Kowloon, Hong Kong, in 2015. She is currently working towards the M.Phil. degree in electrical engineering with the City University of Hong Kong.

Her research interests include electromagnetic energy harvesting, maximum power point tracking, and impedance matching.

Henry Shu-hung Chung (Fellow, IEEE) received the B.Eng. and Ph.D. degrees in electrical engineering from Hong Kong Polytechnic University, Kowloon, Hong Kong, in 1991 and 1994, respectively.

Since 1995, he has been with the City University of Hong Kong, Kowloon, where he is currently a Professor with the Department of Electronic Engineering, and the Director of the Center for Smart Energy Conversion and Utilization Research. He has edited one book, authored eight research book chapters and over 460 technical papers including 200 refereed journal papers in his research areas, and holds 50 patents. His research interests include renewable energy conversion technologies, lighting technologies, smart grid technologies, and computational intelligence for power electronic systems.

Dr. Chung was the Chair of the Technical Committee of the High-Performance and Emerging Technologies, IEEE Power Electronics Society in 2010–2014. He is currently an Associate Editor of the IEEE TRANSACTIONS ON POWER ELECTRONICS and the IEEE JOURNAL OF EMERGING AND SELECTED TOPICS IN POWER ELECTRONICS. He was Editor-in-Chief of the IEEE Power Electronics Letters 2014–2018. He was the recipient of the numerous industrial awards for his invented energy saving technologies.

Authorized licensed use limited to: Chulalongkorn University provided by UniNet. Downloaded on August 25,2020 at 06:24:19 UTC from IEEE Xplore. Restrictions apply.